Article

Cancer Cell

Oncolytic Virus-Mediated Targeting of PGE_2 in the Tumor Alters the Immune Status and Sensitizes Established and Resistant Tumors to Immunotherapy

Graphical Abstract

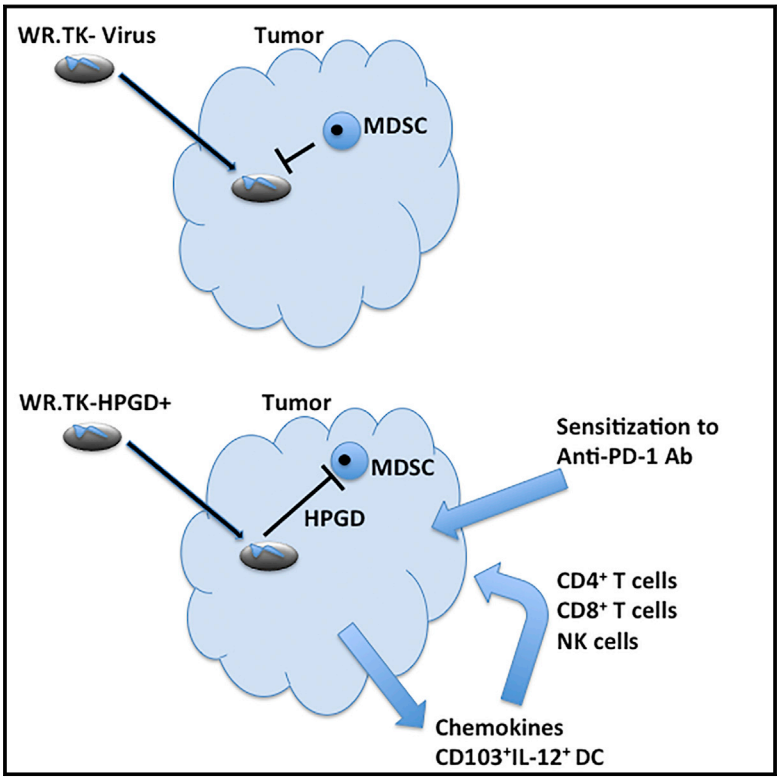

Highlights

- Identification of granulocytic MDSC as key mediators of resistance to immunotherapy
- Oncolytic virus-expressed HPGD targets PGE_2 and depletes G-MDSC in the tumor
- Reduction in PGE_2 in the tumor alters chemokine profiles and immune cell infiltrate
- Targeting of PGE_2 sensitizes established and resistant tumors to imnmunotherapies

Authors

Weizhou Hou, Padma Sampath, Juan J. Rojas, Steve H. Thorne

Correspondence

thornesh@upmc.edu

In Brief

Hou et al. identify the prostaglandin PGE_2 in the tumor as a key mediator of resistance to immunotherapies, including oncolytic virotherapy. Viral vectors engineered to target PGE_2 are capable of overcoming localized immunosuppression to allow for robust anti-tumor adaptive immune responses.

Hou et al., 2016, Cancer Cell *30*, 108–119
July 11, 2016
http://dx.doi.org/10.1016/j.ccell.2016.05.012

CellPress

Cancer Cell
Article

Oncolytic Virus-Mediated Targeting of PGE_2 in the Tumor Alters the Immune Status and Sensitizes Established and Resistant Tumors to Immunotherapy

Weizhou Hou,[1] Padma Sampath,[1] Juan J. Rojas,[1] and Steve H. Thorne[1,2,*]
[1]Department of Cell Biology, University of Pittsburgh Cancer Institute, University of Pittsburgh, Pittsburgh, PA 15213, USA
[2]Department of Immunology, G17a, Hillman Cancer Center, University of Pittsburgh, 5117 Center Avenue, Pittsburgh, PA 15213, USA
*Correspondence: thornesh@upmc.edu
http://dx.doi.org/10.1016/j.ccell.2016.05.012

SUMMARY

Immunotherapies are highly promising cancer treatments, but understanding the factors mediating their resistance remains critical. Successes in randomized clinical testing have supported the growing appreciation that oncolytic virotherapies primarily act as immunotherapies. Here we identified prostaglandin E2 (PGE_2) in the tumor as a key mediator of resistance to immunotherapies, including oncolytic vaccinia virotherapy. Elevated levels of PGE_2 coupled to suppressive chemokine profiles and high levels of granulocytic myeloid-derived suppressor cells resulted in loss of immunotherapeutic potential. Viral vectors engineered to target PGE_2 were capable of overcoming localized immunosuppression leading to profound changes in the tumor's immune status. This allowed the viral vectors to raise robust antitumor adaptive immune responses and sensitized established and previously resistant tumors to immunotherapies.

INTRODUCTION

Recent clinical successes have focused interest on the potential of cancer immunotherapies. However, solid tumors often display the capacity to limit immune induction or to mediate early immune shutoff both locally and systemically. Identifying the key mediators of resistance to immunotherapy will allow the development of more robust treatments with more predictable responses.

Oncolytic viruses (OVs) are vectors designed to selectively replicate in and destroy cancer cells, and multiple OVs based on many different viral strains are currently undergoing clinical testing. However, notable among the current clinical generation of oncolytic viral vectors is that those that have succeeded in randomized trials have expressed an immune-activating cytokine (granulocyte-macrophage colony-stimulating factor [GM-CSF]) (Andtbacka et al., 2013; Heo et al., 2013). This reinforces a plethora of pre-clinical data indicating that the immune response can be a key mediator of OV activity (Lichty et al., 2014) and has led to the development of several ingenious strategies to enhance the immune-activating potential of OVs (Kottke et al., 2013; Tysome et al., 2012; Zhang et al., 2014). The situation is complex, however, as enhanced immune activation frequently reduces oncolytic activity and other reports have demonstrated that certain immune-suppression strategies can also enhance OV activity (Alvarez-Breckenridge et al., 2012; Chen et al., 2013; Lun et al., 2009). A better understanding of the importance of OV-mediated immunotherapeutic activity, how this interacts with oncolytic activity, and how OVs can be most beneficially engineered to interact with the host immune response is therefore needed.

Multiple OV strains based on vaccinia have been reported (Kirn et al., 2007; Mastrangelo et al., 1999; Thorne et al., 2007; Zhang et al., 2007), and one of these expressing GM-CSF, Pexa-Vec (JX-594), has produced encouraging responses in randomized clinical testing (Heo et al., 2013; Park et al., 2008).

Significance

Cancer immunotherapies, including oncolytic viruses, offer the potential for curative cancer treatments. However, patients often present with a combination of systemic immune defects and localized immunosuppression within the tumor that limit immune activation or mediate premature immune shutoff, leading to resistance. Through identification of critical pathways and immunosuppressive cell lineages mediating resistance to oncolytic viral therapies, it was possible to develop viral vectors to overcome them. As a result, previously resistant cancer models became sensitive to oncolytic viral therapy and other immunotherapies. These findings have the potential to significantly enhance the effectiveness of oncolytic viral and other immunotherapies in the clinic and to delineate approaches to overcome resistance to other cancer therapies.

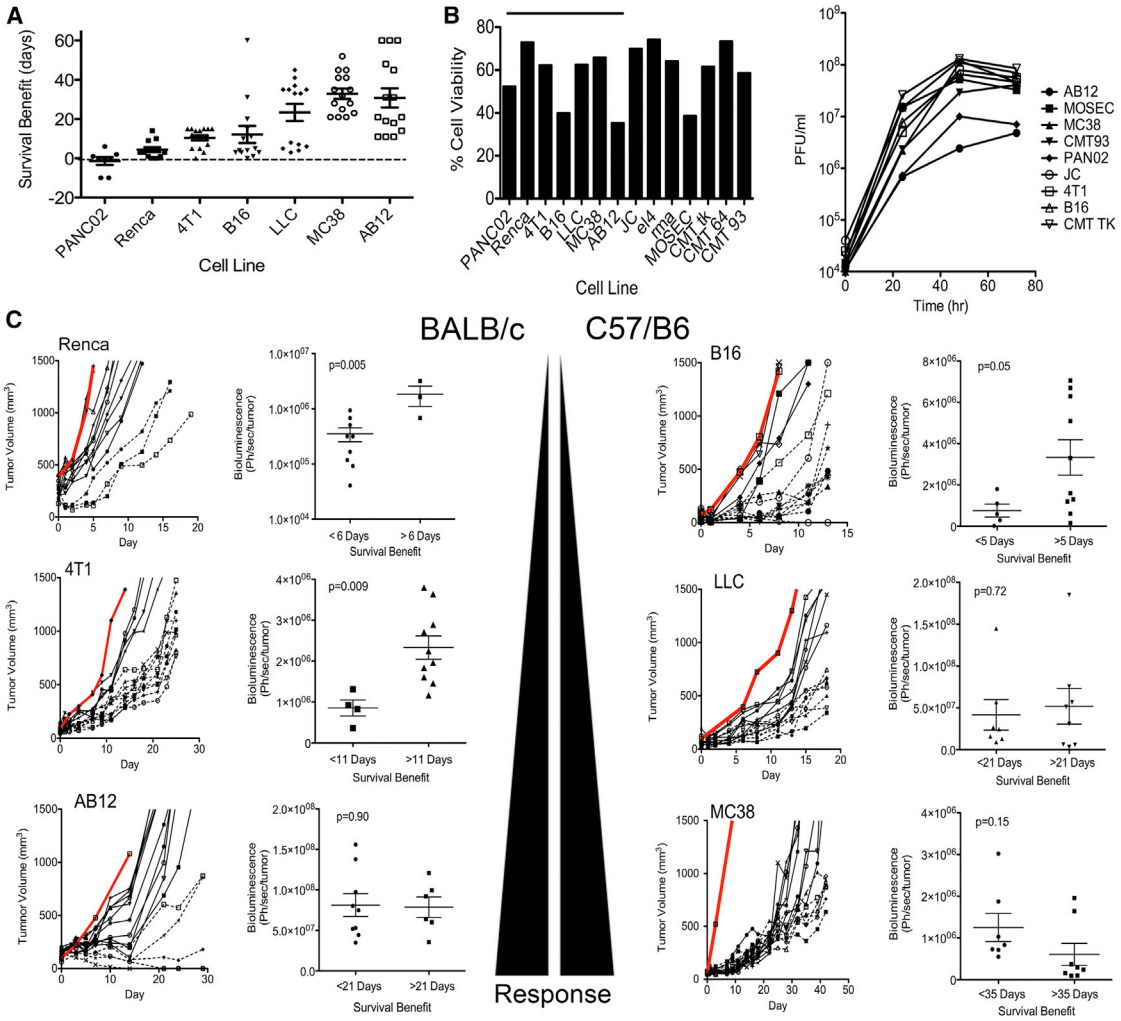

Figure 1. Response to Oncolytic Vaccinia Therapy in Different Immunocompetent Mouse Models

(A) Syngeneic tumors were implanted subcutaneously into BALB/c or C57/BL6 mice and treated with a single intratumoral (i.t.) injection of low dose (1×10^7 plaque-forming units [pfu]) WR.TK$^-$ when tumors reached 50–100 mm^3. Survival benefit (increased survival compared with PBS-treated control mice) was plotted for each tumor model.

(B) Cell viability (left), as determined by MTS assay 72 hr after infection with WR.TK$^-$ at an moi of 1.0 was plotted as percentage viability relative to uninfected cells for indicated mouse tumor cell lines, and viral replication (right) was followed in the same cell lines after the same treatment by plaque assay on BSC-1 cells.

(C) Tumor growth for individual mice treated as in (A) are shown for six of the seven tumor models (PAN02 displayed no survival benefit) and compared with PBS controls (red lines). For each tumor model, individual mice are divided into good responders (dashed lines) or poor responders (solid lines) depending on assigned survival benefits. Bioluminescence imaging was performed at 24 hr post-treatment to measure viral gene expression from within the tumors, and the bioluminescence imaging signal for poor and good responders was normalized to tumor volume and plotted (right-hand graph for each cell line). Error bars ± SEM. See also Figure S1.

However, it is apparent that even in these successful clinical trials, some patients appear resistant to the therapy. It will therefore be critical for the future development of the platform to discover how and why some patient's tumors do not respond, and to develop approaches to overcome this.

Treating different immunocompetent mouse tumor models with oncolytic vaccinia results in a range of in vivo sensitivities, creating an opportunity to interrogate the causes of resistance and to determine the relative importance of immunotherapeutic and oncolytic mechanisms of tumor killing under different conditions. Strategies to overcome the causes of resistance might then be developed.

RESULTS

Immunocompetent Mouse Tumor Models Display Differing Sensitivities and Patterns of Response to Oncolytic Vaccinia Therapy

We initially examined a panel of syngeneic immunocompetent mouse tumor models in order to delineate the mediators of resistance or susceptibility to oncolytic vaccinia therapies. The in vitro sensitivities of 14 different mouse tumor cell lines to viral replication and cell killing were compared with in vivo responses with syngeneic tumors formed from a subset of seven of the same cell lines (Figures 1A and 1B). Mice were treated via direct

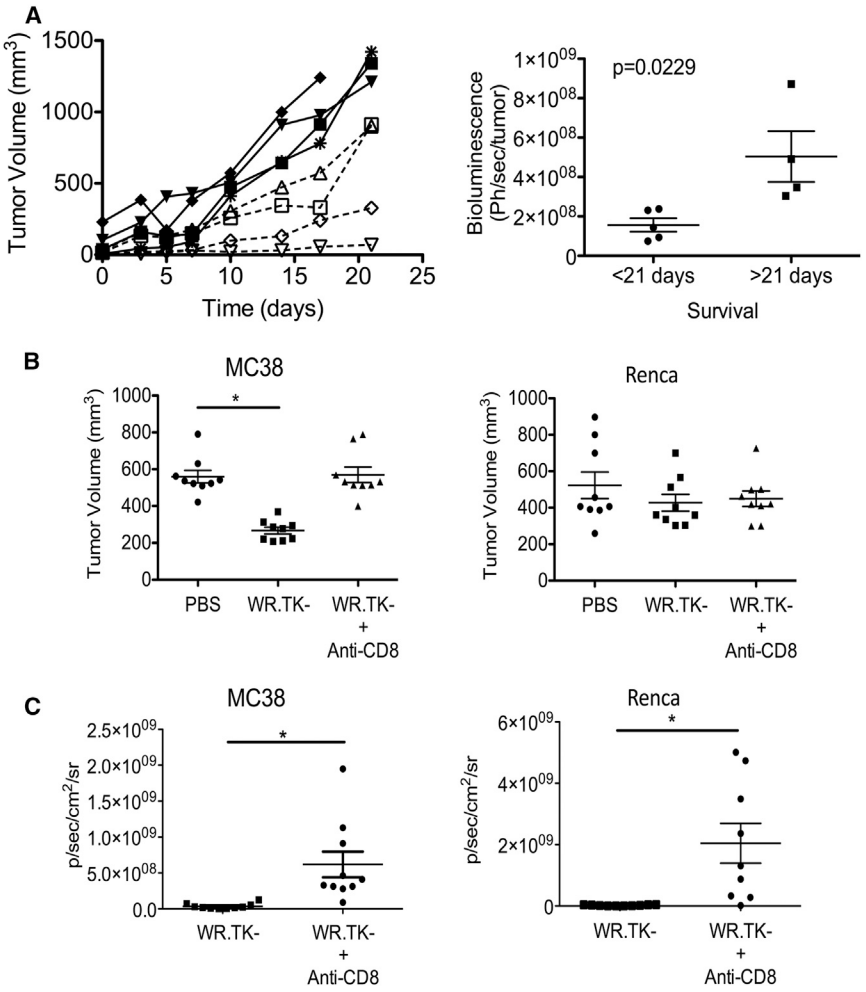

Figure 2. Role of Immune Response in the Therapeutic Effect of Oncolytic Vaccinia

(A) LLC tumors were implanted into NOD SCID mice and tumor growth for individual mice is shown over time after treatment with 1×10^7 pfu WR.TK$^-$ (left). These were divided into good (dashed lines) and poor (solid lines) responders, and bioluminescence imaging used to determine viral luciferase transgene expression from the tumor at different times after treatment (right).

(B) MC38 and Renca cells were implanted subcutaneously into syngeneic mice and treated with WR.TK$^-$ (1×10^7 pfu i.t.) after antibody depletion of CD8$^+$ cells from the mice. *$p < 0.05$.

(C) The viral gene expression from the tumor in the same mice as in (B) was followed by bioluminescence imaging at day 3 after treatment. *$p < 0.05$. Error bars ± SEM. See also Figure S2.

intratumoral (i.t.) injection of a low dose of viral therapy to remove any variability due to differences in systemic delivery. No correlation was seen between viral replication or viral-mediated cell killing in vitro and in vivo anti-tumor effects, indicating factors in addition to direct oncolytic activity may be primarily responsible for optimal therapeutic benefit.

Oncolytic vaccinia strain WR.TK$^-$Luc$^+$ was used during these initial experiments. This virus bears the same thymidine kinase (TK) deletion as all three oncolytic vaccinia strains currently in the clinic (Kim et al., 2006; McCart et al., 2001; Worschech et al., 2009; Zeh et al., 2014) and expresses luciferase so that viral gene expression levels could be quantified over time in individual mice (as a surrogate for viral replication and persistence), and compared with subsequent response. It was noted that two distinct kinetic patterns of viral gene expression emerged in vivo (Figure 1C). In the more resistant tumor models (defined as those in which viral therapy increased overall survival by less than 2 weeks, as seen with PANC02, Renca, 4T1, and B16; Figure 1A), the level of viral gene expression measured from within the tumor at 24 hr after delivery correlated closely with subsequent response (Figure 1C). Therefore, within any one of these resistant tumor models, greater initial infection and early replication in the tumor (early viral gene expression) results in improved subsequent response. This pattern would be predicted if viral replication was the key mediator of therapeutic effect and suggests that the limited response seen in the more resistant tumor models is primarily due to oncolytic activity.

However, a different pattern was noted in the tumor models that were more susceptible to viral therapy (LLC, MC38, and AB12) (Figures 1A and 1C). In these models, there was no correlation between early viral gene expression in the tumor (at 24 hr after treatment) and subsequent response. Instead, the best responders within each of the sensitive tumor models demonstrated a trend toward a more rapid and robust clearance of the virus, as seen with reduced levels of viral gene expression in the tumor at 4 or 5 days after treatment (Figure S1). This robust viral clearance might indicate that a strong immune response is being induced within the tumor that reinforces any direct oncolytic effects in the more sensitive tumor models.

Several lines of evidence supported the above hypothesis. Firstly, when LLC tumors were implanted into immunodeficient mice, the viral gene expression pattern changed to match that of the poor responders (oncolytic activity only), with viral bioluminescence within the tumor at 24 hr correlating with subsequent response (Figure 2A). Of note, when LLC tumors implanted into immunodeficient mice were treated, most of the tumors displayed a pattern of short-term stable disease (for 10–15 days) followed by progression (Figure 2A); this is despite evidence of ongoing viral replication (luciferase gene expression) in the tumor (Figure S2). However, when the same tumor model was implanted and treated in immunocompetent mice (Figure 1C), 50% of the animals (6 of 12) displayed longer-term (>21 days) stabilization of tumor growth despite the fact that the viral therapy was cleared within 10 days of treatment (Figure S2). Secondly, anti-CD8 antibody was used to deplete CD8$^+$ cells from both sensitive (MC38) and resistant (Renca) tumor models (Figure 2B). Depletion of CD8$^+$ T cells significantly reduced the vector's therapeutic activity in the sensitive MC38 tumor model,

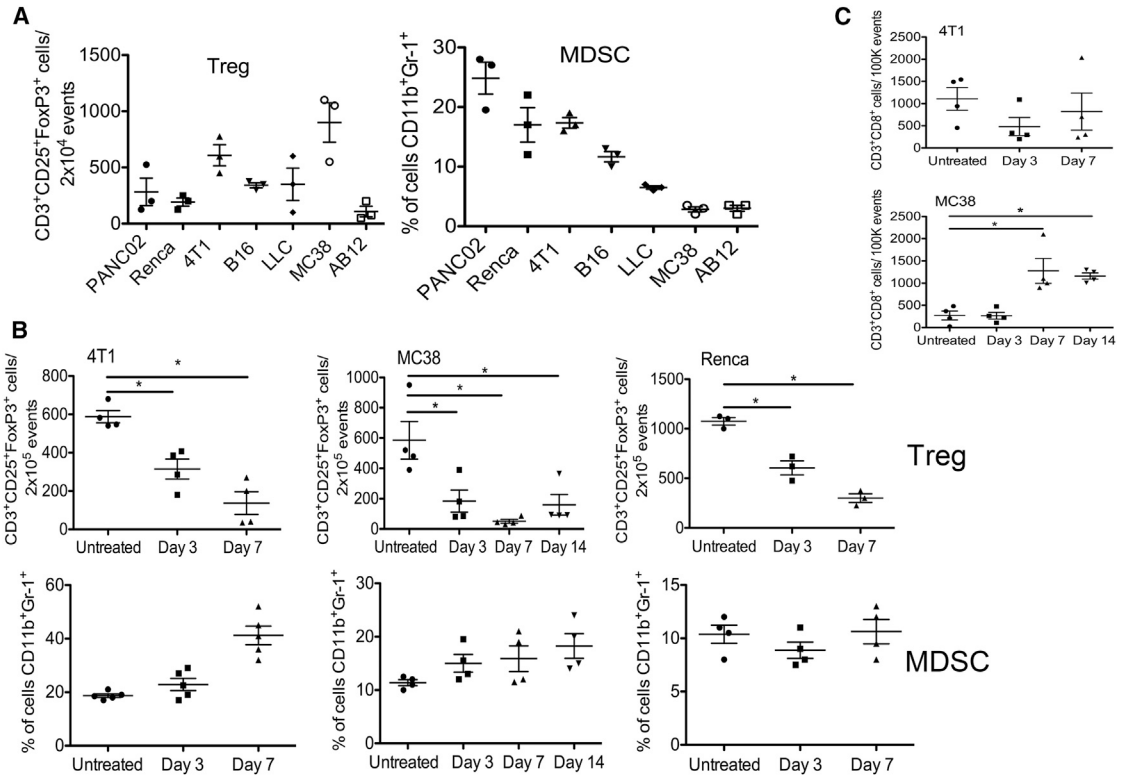

Figure 3. Resistance of Different Tumor Models to Oncolytic Viral Therapy Is Mediated by Localized Immune Suppression within the Tumor

(A) Baseline levels of regulatory T cells (Treg) and monocyte-derived suppressor cells (MDSC) in tumors before therapy. Syngeneic subcutaneous tumors were formed from different cell lines and mice killed when the tumors reached 100–200 mm^3, and the tumors disaggregated. Flow cytometry was used to quantify the relative levels of Treg ($CD3^+CD25^+FoxP3^+CD8^-$) and MDSC ($CD11b^+Gr\text{-}1^+$) in the tumors.

(B) Effect of viral therapy on suppressive immune cell profile within the tumor. Tumor-bearing mice were treated with a single low dose (1×10^7 pfu) i.t. injection of $WR.TK^-$ and the levels of Treg and MDSC in the tumors at different times after treatment were analyzed as in (A).

(C) $CD3^+CD8^+CD4^-$ T cells were also quantified in the tumor as in (A). (*$p < 0.05$). Error bars ± SEM. See also Figures S3 and S4.

but had no effect in Renca, further supporting the hypothesis that the resistant tumor models were unable to mount a robust immunotherapeutic response. Of note, the reduced therapeutic activity in MC38 tumors after $CD8^+$ depletion occurred despite increased viral replication (Figure 2C), again highlighting the increased importance of immunotherapeutic over oncolytic activity in these vectors.

Resistance to Viral Therapy Correlated with MDSC in the Tumor Environment

It appears, therefore, that in order to produce a significant therapeutic effect, the viral vector needs to be able to mediate both an oncolytic and immunotherapeutic response, while resistant tumors were able to limit this to an oncolytic-mediated response only. The immune response to viral therapy was therefore examined in more detail in order to define differences between susceptible and resistant tumors.

It was determined that pS6 levels were reduced systemically in myeloid dendritic cells (DCs) in tumor-bearing animals, and that this reduction was more pronounced in the resistant tumor-bearing mouse models (Figure S3A), indicating that a defect in or suppression of the DC response may be important for resistance to immunotherapy in these tumors. However, because oncolytic viral immune activation is likely to primarily occur subsequent to replication in the tumor, the condition of the more localized immune environment within the tumor was examined. Different immune cells are associated with a suppressive phenotype, including myeloid-derived suppressor cells (MDSC) and regulatory T cells (Tregs), and so the overall level of these different cell types in both the spleen and the tumor of the same seven mouse tumor models were determined prior to therapy. It was observed that the overall level of MDSC found in the tumor for different tumor models correlated very closely with the resistance or sensitivity of that model to subsequent viral therapy (Figures 3A and S3B). No similar correlation was seen with Treg levels or with either cell type in the spleen (Figures 3A and S3C).

We further examined what changes occurred in the tumor after viral therapy and saw that, for different tumor models (4T1, MC38, and Renca, Figure 3B), the addition of vaccinia therapy resulted in a rapid loss of Treg, but that MDSC levels were unaffected (and actually continued to increase over time, as they also did in control groups). It therefore appears that MDSC are unaffected by the presence of oncolytic vaccinia and high levels of MDSC can block the immunotherapeutic activity of these vectors. Of note, in the sensitive MC38 tumor model (with lower background levels of MDSC), the viral therapy was actually found to significantly increase the number

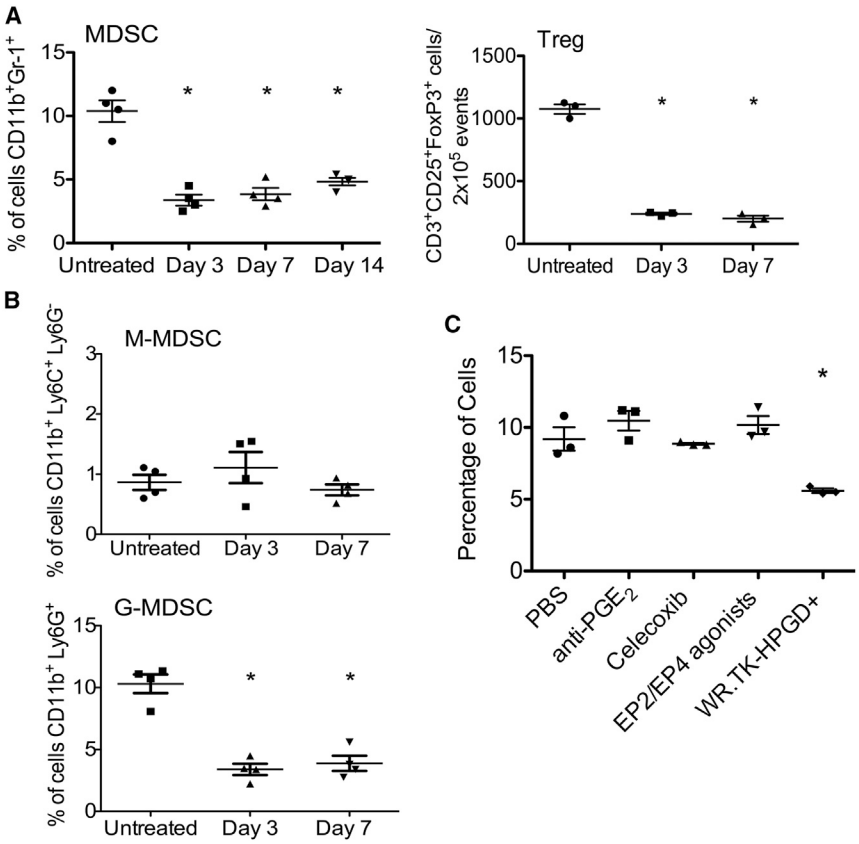

Figure 4. HPGD Expression from Oncolytic Vaccinia Reduces MDSC in the Tumor

(A) Mice bearing Renca tumors were treated with a low dose (1×10^7 pfu) i.t. injection of WR.TK$^-$.HPGD$^+$ and killed at the indicated times, tumors recovered, disaggregated, and analyzed by flow cytometry as in Figure 3. *$p < 0.05$ compared with control.

(B) Cells as in (A) were additionally stained for Ly6G and Ly6C to distinguish effects on monocytic MDSC (M-MDSC) (CD11b$^+$Ly6C$^+$Ly6G$^-$) and granulocytic MDSC (G-MDSC) (CD11b$^+$Ly6G$^+$) in the tumor.

(C) G-MDSC levels in the tumors for mice treated as in (A) and killed after 3 days were compared with mice treated with PBS, anti-PGE_2 antibody, celecoxib, or EP2/4 agonists. All non-viral treatments were administered daily for 3 days. Error bars ± SEM. See also Figure S5.

of CD8$^+$ T cells present in the tumor, an indication of immunotherapeutic activity, whereas the more resistant 4T1 tumor model (with higher baseline MDSC levels) did not display any significant increase in CD8$^+$ T cells in the tumor after treatment (Figure 3C).

We have recently described an oncolytic vaccinia strain, WR.B18R$^-$IFNβ$^+$, with enhanced immunotherapeutic effects (Kirn et al., 2007; Wang et al., 2011), while oncolytic viral strains expressing GM-CSF (including vaccinia and herpes-simplex-virus-based strains; Andtbacka et al., 2013; Heo et al., 2013) have produced the most dramatic clinical responses to date despite GM-CSF being associated with MDSC proliferation (Kohanbash et al., 2013). The effects of these immune-enhanced vectors were therefore also examined to see if they were able to overcome MDSC-mediated immunosuppression in the tumor. It was found that the more immunogenic vaccinia strains (WR.TK$^-$mGM-CSF and WR.B18R$^-$mIFNβ$^+$) provided no additional benefit over WR.TK$^-$ in a sensitive tumor model (MC38, Figure S4), with WR.TK$^-$mGM-CSF even increasing MDSC in the tumor. In the resistant tumor model (4T1, Figure S4) all viral treatments resulted in significant increases in MDSC levels in the tumor. This was less dramatic for the immune-enhanced vectors, and correlated with a small but not significant increase in CD8$^+$ T cell infiltration. It therefore appears that the inability of the virus to induce a robust immunotherapeutic effect in tumors with high levels of MDSC is a critical determinant of resistance and cannot be overcome by increasing viral-mediated immune activation.

Targeting of PGE_2 Can Reduce MDSC and Re-sensitize Resistant Tumors to Viral Therapy

Recent reports have identified cyclooxygenase (COX-2)-mediated production of prostaglandin E2 (PGE_2) as a key determinant of MDSC tumor infiltration and maintenance of the suppressive phenotype in these cells (Donkor et al., 2009; Fujita et al., 2011; Kalinski, 2012; Obermajer et al., 2011a, 2011b; Rodriguez et al., 2005). It was noted that viral therapy did not significantly alter the overall levels of COX-2 expression in the tumor (Figure S5A).

We therefore looked to develop approaches to reduce PGE_2 levels, including addition of the COX-2 inhibitor celecoxib or viral expression of the prostaglandin-inactivating enzyme hydroxyprostaglandin dehydrogenase 15-(NAD) (HPGD) (Figures S5B and S5C). Initial in vitro experiments determined that, even when used at levels known to be toxic in vivo, celecoxib was unable to reduce PGE_2 levels by the amounts achieved with HPGD expression (Figure S5D). Oncolytic vaccinia expressing HPGD (WR.TK$^-$HPGD$^+$) was therefore tested in several different mouse tumor models.

It was found that WR.TK$^-$HPGD$^+$ was non-toxic and that the numbers of MDSC cells in Renca (resistant) tumors were rapidly and significantly reduced after treatment with WR.TK$^-$HPGD$^+$ (Figure 4A). Interestingly, WR.TK$^-$HPGD$^+$ also induced a more rapid and robust reduction in Treg numbers in the tumor. Because several subsets of MDSC have been defined in mice, we further looked to determine if the monocytic MDSC (CD11b$^+$Ly6G$^-$Ly6C^{hi}) and granulocytic MDSC (G-MDSC) (CD11bLy6G$^+$Ly6C^{Lo}) were equally targeted. It was found that HPGD expression selectively depleted the G-MDSC population (Figures 4B and S5E) that is typically found in greater numbers and thought to be terminally differentiated.

The identification of the COX-2-PGE_2 pathway as a key mediator of immunosuppression has led to a variety of inhibitory approaches being proposed. We therefore compared the in vivo effects of different COX-2 or PGE_2 inhibitors on the levels of

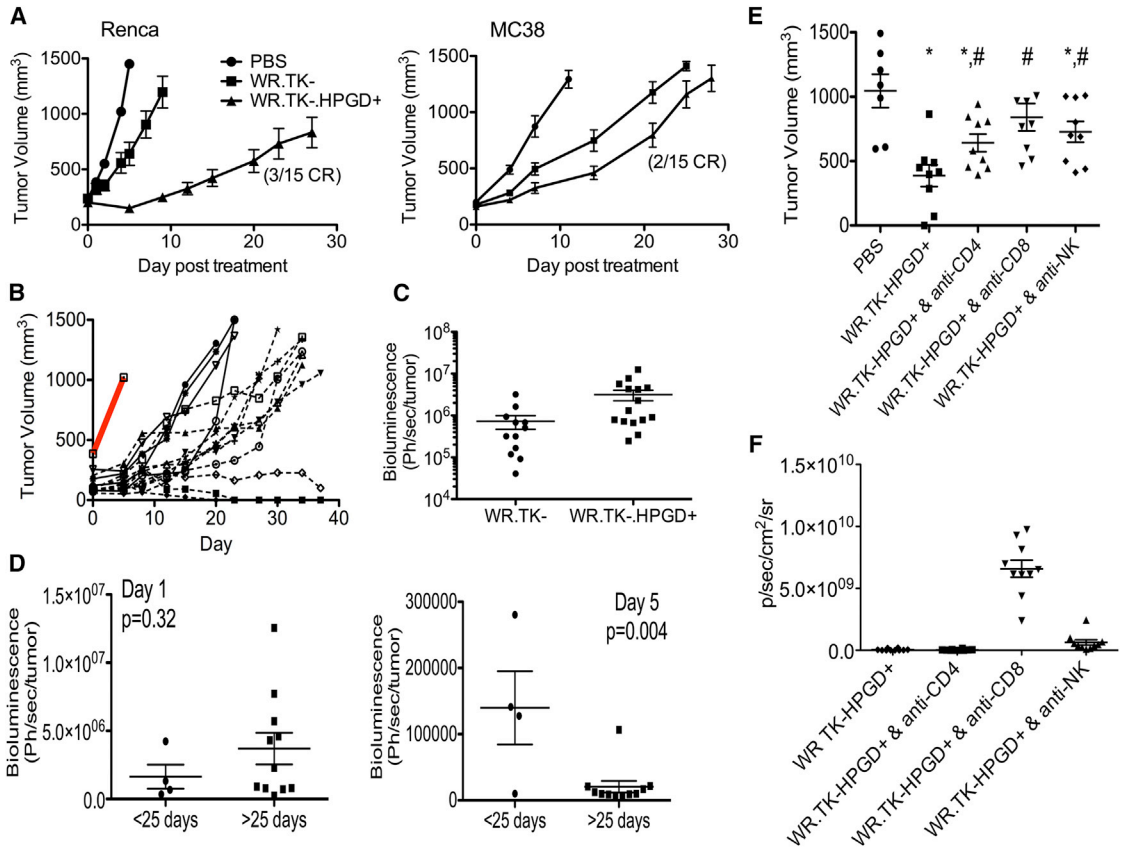

Figure 5. Enhanced Therapeutic Activity of WR.TK⁻.HPGD⁺

(A) Mice bearing subcutaneous Renca or MC38 tumors were treated with a single i.t. injection of PBS or 1 × 10^7 pfu of WR.TK⁻ or WR.TK⁻HPGD⁺, and subsequent tumor growth followed by caliper measurement (n = 15 per group).

(B) Renca tumor growth in individual mice treated with WR.TK⁻HPGD⁺ is plotted, compared with PBS control (red bar), and divided into good (solid line) and best (dashed line) responders.

(C) The viral gene expression (bioluminescence) from the tumor at 24 hr after therapy was compared for mice treated with WR.TK⁻ and WR.TK⁻HPGD⁺.

(D) The bioluminescence signal (viral gene expression) from the tumors of mice treated with WR.TK⁻HPGD⁺ at days 1 and 5 were normalized to tumor volume and shown for both good and best responders.

(E) The role of different immune subsets in the increased therapeutic activity of WR.TK⁻HPGD⁺ in Renca tumors was examined through depletion of CD4⁺, CD8⁺, and NK cells (*p < 0.05 versus PBS; #p < 0.05 versus WR.TK⁻HPGD⁺).

(F) Viral gene expression from the tumor (bioluminescence imaging) at day 3 after treatment of immune cell-depleted mice. Error bars ± SEM. See also Figure S6.

G-MDSC in the tumor, including PGE_2-depleting antibody, celecoxib, and agonists of the PGE_2 receptors EP2 and EP4. The only approach capable of reducing G-MDSC levels was WR.TK⁻HPGD⁺ (Figure 4C), indicating that high-level HPGD expression from within the tumor is uniquely able to break this immunosuppressive cycle.

These alterations in the tumor microenvironment further correlated with an enhanced therapeutic effect in different mouse tumor models (Figure 5A). Of note, the Renca tumor model that was previously resistant to viral therapy (displaying an "oncolytic only" phenotype and high baseline levels of MDSC) displayed the greatest increase in therapeutic benefit after HPGD transgene expression (Figures 5A and 5B). However MC38 tumors that had low-level baseline MDSC and already displayed sensitivity to therapy also showed a significant further therapeutic advantage after treatment with WR.TK⁻HPGD⁺.

The patterns of viral luciferase transgene expression were also compared for WR.TK⁻ and WR.TK⁻HPGD⁺ in the previously resistant Renca tumor model (Figures 1B, 5C, and 5D). Interestingly, it was initially noted that, unlike many immune-enhancing transgenes, HPGD expression did not reduce the initial replicative capability of the virus (Figures 5C and S6). However, the virus was cleared from the tumor slightly faster with HPGD expression than for WR.TK⁻ alone, again indicative of the raising of a robust immune response. It was also seen that whereas WR.TK⁻ treatment displayed the "oncolytic only" phenotype (with higher gene expression at day 1, correlating with greatest subsequent therapeutic benefit) (Figure 1B), WR.TK⁻HPGD⁺ treatment of the same tumor model displayed the "oncolytic plus immunotherapeutic" phenotype, with the best responders displaying a robust and rapid clearance of the virus at day 5 after treatment (Figure 5D). This was further explored through depletion of different immune subsets from the mice before treatment with WR.TK⁻HPGD⁺ (Figure 5E). It was noted that depletion of CD8⁺ cells had the most profound effect, resulting in a loss of significance in the therapeutic benefit after treatment. However

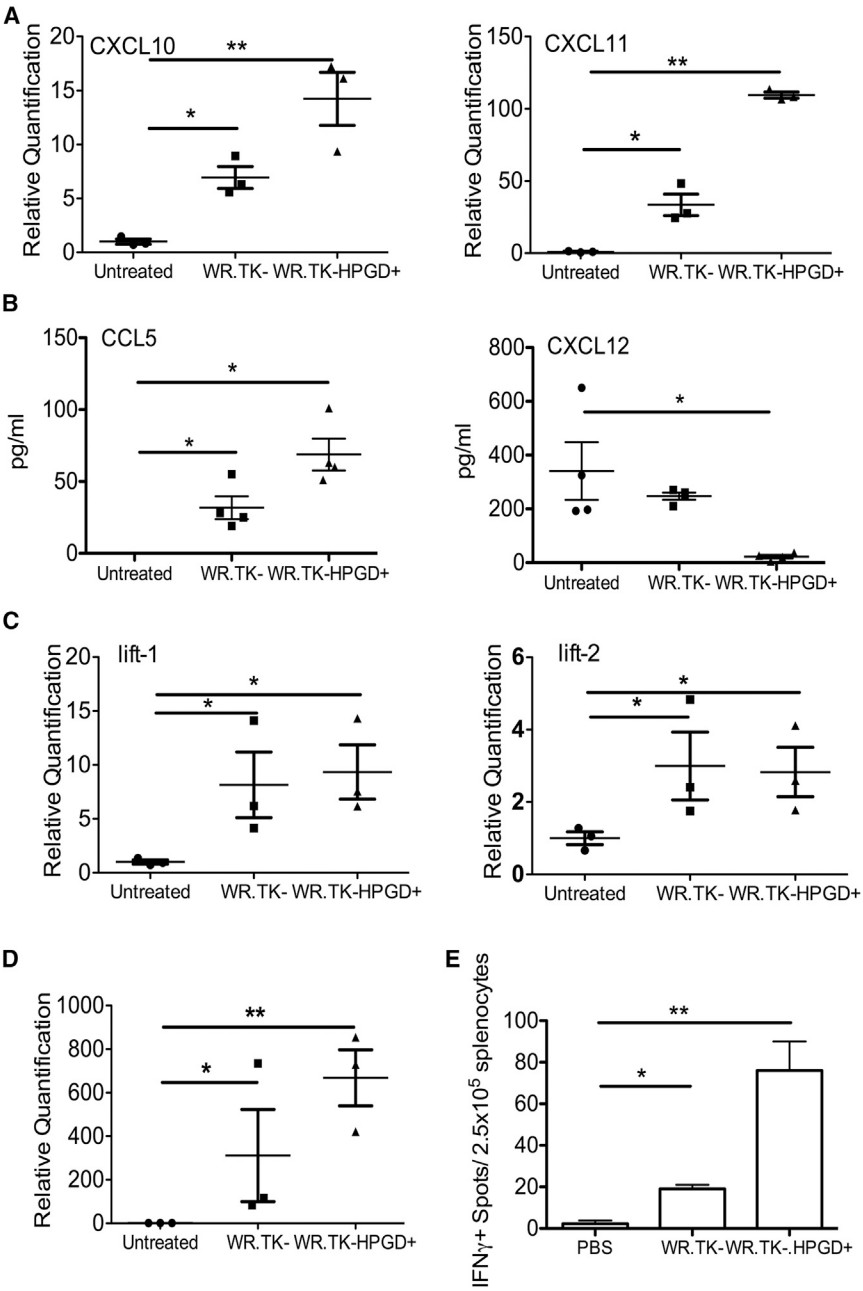

Figure 6. HPGD Expression Enhances the Immune Response within and against the Tumor

(A) Mice bearing Renca tumors were treated as indicated with 1×10^7 pfu of different viral strains i.t. and killed after 3 days. qRT-PCR was used to detect the expression of CXCL10 and CXCL11 in the tumor.

(B) ELISA was used to detect the levels of CCL5 and CXCL12 in the serum of mice in (A) at the same times (below limits of detection).

(C) Innate (type I IFN) immune response of mice as in (A) was determined by qRT-PCR of lift-1 and lift-2.

(D) Adaptive immune response, as measured by qRT-PCR of IFNγ was determined for mice as in (A).

(E) Anti-tumor CTL response was determined in splenocytes collected form Renca tumor-bearing mice 7 days after the indicated treatments.

Anti-tumor CTL response was determined by ELISPOT (*$p < 0.05$, **$p < 0.001$). Error bars ± SEM.

both $CD4^+$ and natural killer (NK) cells also appear to be important, as their depletion resulted in a significant reduction in therapeutic effect (even though $WR.TK^-HPGD^+$ treatment maintained a significant therapeutic benefit). It therefore appears that HPGD expression, in addition to depleting G-MDSC, is capable of inducing further immunotherapeutic benefits.

We looked to define in more detail the mechanisms underlying the therapeutic advantage seen with $WR.TK^-HPGD^+$. It was noted that at 3 days after treatment, $WR.TK^-$ alone was able to modestly increase the levels of several Th1-associated chemokines both systemically and in the tumor (Figures 6A and 6B). The expression of HPGD, however, produced significant further increases and was also capable of significantly reducing the level of the suppressive chemokine CXCL12 (SDF-1), which is associated with MDSC attraction into the tumor, tumor metastasis, and a poor prognosis (Chatterjee et al., 2014; Obermajer et al., 2011b) (Figure 6B). Further analyses looked at the levels of selected cytokines and inflammatory pathways within the tumor. As expected, $WR.TK^-$ infection resulted in an increase in the type I interferon (IFN) response, seen with increased lift-1 and lift-2 expression (Figure 6C). However, this was not increased further with HPGD expression, indicating that HPGD does not enhance the innate immune response that might be expected to reduce viral oncolytic effects and mediate premature viral clearance from the tumor. Instead, HPGD expression significantly increased the level of IFNγ produced within the tumor (Figure 6D). Oncolytic viral infection alone, therefore, appears capable of inducing an inflammatory response and initial immune activation, whereas HPGD expression may be required to prevent premature shutdown of the immune response before full induction of adaptive immunity. This is supported by the observation that at 7 days after treatment $WR.TK^-HPGD^+$ had induced a 4-fold increase in the number of anti-tumor cytotoxic T lymphocytes (CTLs) in the spleen relative to $WR.TK^-$ treatment (Figure 6E).

$WR.TK^-HPGD^+$ Can Enhance Sensitivity of Resistant Tumors to Other Immunotherapies

The observed changes in the tumor's chemokine profile may be responsible for enhancing the CTL response through mediating changes in the immune cell repertoire within the tumor. This

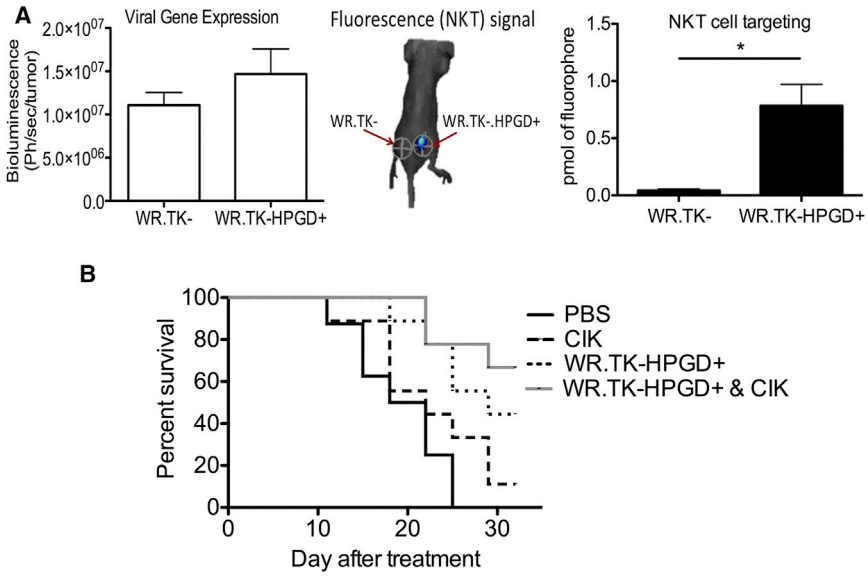

Figure 7. Enhanced Therapeutic Effects of Combination with Adoptive T Cell Transfer

(A) Mice were implanted bilaterally with Renca tumors. When tumors reached 50–100 mm^3, the tumor on one flank was injected with 1×10^7 pfu of WR.TK$^-$ and the tumor on the opposite flank was injected with WR.TK$^-$HPGD$^+$. After 24 hr 1×10^7 activated and Cy5.5-labeled NKT (CIK) cells were delivered via tail vein injection. 24 hr later mice were imaged for bioluminescence to measure viral gene expression and fluorescence to determine NKT cell trafficking to tumors (*$p < 0.05$). A representative example of fluorescence imaging is shown.

(B) BALB/c mice with subcutaneous Renca tumors were treated with PBS, 1×10^7 pfu of WR.TK$^-$HPGD$^+$ (i.t.), 5×10^6 CIK cells (intravenous), or both therapies on the same day. Animal survival, taken as time to tumor burden reaching 1,000 mm^3, was determined by caliper measurement. Error bars ± SEM.

might further provide benefits for attracting therapeutic T cells into the tumor after adoptive T cell transfer or application of a therapeutic vaccine. This was examined using a bilateral Renca tumor model, whereby one tumor was injected with WR.TK$^-$ while the tumor on the opposite flank was injected with WR.TK$^-$HPGD$^+$. It was seen that activated NK T (NKT) cells (cytokine-induced killer [CIK] cells) delivered intravenously, trafficked significantly more efficiently to the HPGD expressing tumor (Figure 7A). This indicates that the expression of HPGD not only limits the suppressive environment within the tumor, but is also capable of enhancing systemic attraction of T cells.

It was seen that CIK cells, used as a model of adoptive T cell transfer (Figure 7B), only had a small therapeutic effect in Renca tumor models, but when combined with WR.TK$^-$HPGD$^+$ they increased survival relative to either treatment used alone.

Perhaps more dramatic was the observed effects of combining WR.TK$^-$HPGD$^+$ with blockade of immune checkpoint inhibitor using anti-PD-1 (Figure 8A). This antibody is known to have no effect in the Renca tumor model (Masters et al., 2014), as was confirmed here, yet combination with WR.TK$^-$HPGD$^+$ produced a large therapeutic advantage, again indicating that WR.TK$^-$HPGD$^+$ has the potential to sensitize otherwise resistant tumors to different immunotherapies. Of particular note, it has recently been reported that aspirin could be used to block COX-2 activity and sensitize tumors to anti-PD-1 therapy (Zelenay et al., 2015); however, this was only possible when the drugs were added before formation of established tumors. In the Renca model used here a similar result is seen (Figure 8A), with anti-PD-1 and aspirin added 3 days after tumor implantation producing a small but significant therapeutic benefit, whereas either used alone had no effect, even at this early time. However, if this same combination is added at later time points, after tumor formation (10 days after tumor implantation), there is no therapeutic benefit. However addition of anti-PD-1 in combination with WR.TK$^-$HPGD$^+$ produces highly significant therapeutic effects, even when these are added at late times to established tumors. Also of note is the observation that adding aspirin to WR.TK$^-$ produced no therapeutic benefit, indicating that aspirin could not substitute for HPGD expression.

The effects of aspirin on sensitizing tumors to anti-PD-1 treatment when added before tumor formation were further examined in (Zelenay et al., 2015) using COX-2-deficient *Ptgs1*$^{-/-}$*Ptgs2*$^{-/-}$ mice, and a role for IL-12p40$^+$CD103$^+$ DC was identified in mediating anti-tumor immunity. These cells were depleted when PGE_2 was present in wild-type mice. Here we found that expression of HPGD from an oncolytic vaccinia could disrupt PGE_2 activity sufficiently, even in established tumors, to induce significant numbers of IL12p40$^+$CD103$^+$ DC in the draining lymph nodes of treated tumors (Figure 8B). A small, but significant increase was seen even with WR.TK$^-$ treatment alone, but the effects were increased significantly when HPGD was also expressed.

DISCUSSION

A variety of approaches have been proposed to overcome the immunosuppressive microenvironment in large solid tumors, with the COX-2-PGE_2 pathway as a key mediator of this suppressive activity. This pathway is an attractive target as it has been associated with attracting and maintaining the suppressive phenotype of MDSC. Breaking this cycle might even allow these suppressive cells to differentiate into an immune-activating phenotype. Here we demonstrated that an oncolytic vaccinia virus expressing the PGE_2-inactivating enzyme HPGD is able to significantly reduce levels of G-MDSC within the tumor. Of several approaches known to target COX-2-PGE_2, WR.TK$^-$HPGD$^+$ was the only one able to actually reduce MDSC levels.

This appears to be especially important in the context of oncolytic viral therapy because the level of MDSC in the tumor at baseline was inversely related to the sensitivity of the tumor to oncolytic vaccinia therapy. Higher levels of MDSC in the tumor suppressed the immunotherapeutic activity of the virus, limiting its activity to oncolytic-mediated cell killing. Although vaccinia has a known capacity to produce a fast-spreading and highly

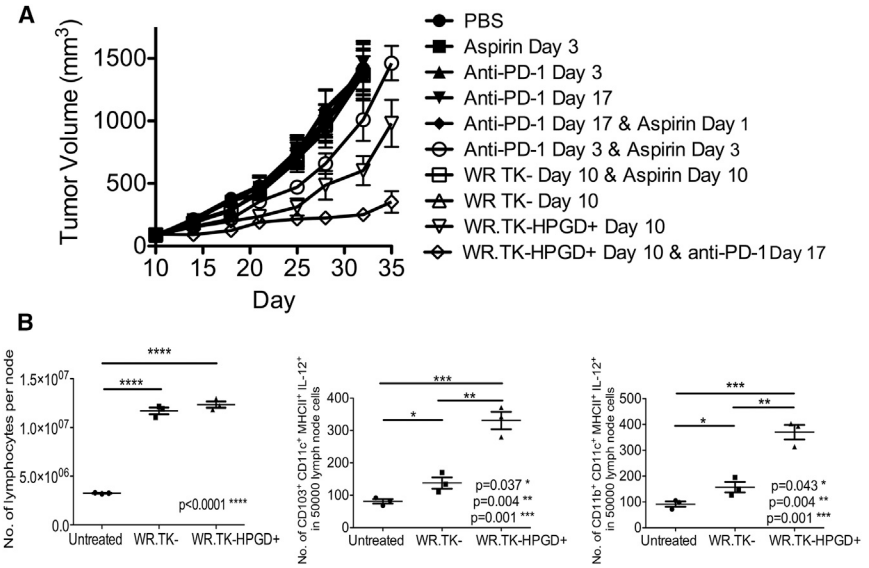

Figure 8. WR.TK$^-$HPGD$^+$ Also Sensitizes Tumors to Anti-PD-1 Therapy

(A) Combination of different viruses with anti-PD-1 antibody is compared with combinations with aspirin, and with aspirin + anti-PD-1 after treatment in BALB/c mice bearing subcutaneous Renca tumors (N.B. the indicated days of treatment are days after tumor implantation). Viruses (WR.TK$^-$ or WR.TK$^-$HPGD) were given as single i.t. doses of 1 × 10^7 pfu; anti-PD-1 antibody (applied twice weekly for 21 days after start of treatment); and aspirin (600 μg/ml provided continuously in drinking water).

(B) Draining lymph nodes were collected 5 days after treatment of mice as in (A) and dissociated for determination of total number of lymphocytes (left), number of CD103$^+$CD11c$^+$MHCII$^+$ IL-12$^+$ cells (center), and number of CD11b$^+$ CD11c$^+$MHCII$^+$ cells (right) per 5,000 events. Error bars ± SEM.

lytic infection in humans or non-human primates (Naik et al., 2006), it is apparent that the immune response plays a more critical role for therapeutic activity, as confirmed here. The determination that local rather than systemic immune suppressive activity is key in preventing viral immunotherapeutic action allows the creation of vectors such as WR.TK$^-$HPGD$^+$ that express transgenes to overcome this suppression locally within the tumor.

Recent clinical success using antibodies that block immune checkpoint inhibitors, such as anti-CTLA-4, anti-PD-1, and anti-PD-L1 (Leach et al., 1996; Topalian et al., 2012; Yuan et al., 2008), have revealed the importance of overcoming the tumor's capacity to prematurely shutdown or curtail an immune response. It is apparent that a successful therapeutic strategy would require both activation of the immune response and prevention of its early shutdown. As such, it is interesting that the standard oncolytic vaccinia strain (WR.TK$^-$) and several immune-enhanced strains (including WR.TK$^-$mGM-CSF) are capable of inducing inflammation at early times, even in resistant tumor models, but were unable to subsequently prime high-level anti-tumor adaptive immunity (in tumors with high baseline G-MDSC).

The expression of HPGD from oncolytic vaccinia, however, produces a vector that is capable of both immune activation and limiting premature immune shutdown in the tumor. The primary mediator of early immune shutdown and suppression after viral therapy appeared to be the G-MDSC lineage within the tumor and that targeting of the PGE_2 was shown to be a potent strategy to reduce the levels of these cells. This combination of immune activation after local viral replication in the tumor and overcoming of immune suppressive effects though G-MDSC depletion resulted in greatly increased anti-tumor CTL and significantly enhanced therapeutic effects. The greatest therapeutic advantage occurs in the previously resistant tumors, where the viral gene expression pattern switches to that of an "immunotherapeutic" response. This confirms that previously resistant tumors can be sensitized to viral therapy through HPGD transgene expression. It would be predicted that expression of HPGD from immune-enhanced vectors (such as WR.TK$^-$GM-CSF) could further increase their immunotherapeutic potential.

It is also of note that HPGD expression was able to significantly enhance therapeutic activity in already sensitive tumor models (with low baseline G-MDSC levels). In this respect, altered chemokine production patterns and enhanced trafficking of activated T cells to tumors treated with virus-expressing HPGD may play an important therapeutic role.

This multi-faceted targeting of the immunosuppressive microenvironment within the tumor through treatment with WR.TK$^-$HPGD$^+$ was further found to sensitize resistant tumors to other immunotherapies, including adoptive immune cell transfer and immune checkpoint modulation. In particular, it was observed that Renca tumors that are naturally resistant to anti-PD-1 therapy, displayed enhanced sensitivity to anti-PD-1 when anti-PD-1 was applied after WR.TK$^-$HPGD$^+$. Other approaches that target COX-2 activity (such as with aspirin) have also been shown to sensitize mouse tumors to anti-PD-1 therapy; however, this was only possible if both therapies were administered before tumor formation. The WR.TK$^-$HPGD$^+$ virus was the only approach found to be effective against pre-established, large solid tumors.

Finally, the description of distinct tumor response phenotypes to oncolytic viral therapy is also a finding that has direct clinical relevance for the application of OVs and potentially other immunotherapies. Recent clinical demonstrations of the ability to image OV-expressed reporter transgenes in the clinic, such as the sodium-iodide symporter expressed from oncolytic measles virus using SPECT imaging (Penheiter et al., 2011; Russell et al., 2014), opens up the possibility of looking for similar patterns of gene expression and robust early OV clearance in a clinical setting. This might be used to predict clinical responses to oncolytic viral therapies at early time points after treatment, a particular problem for immunotherapies, where tumor swelling often precedes therapeutic response. However, other mechanisms of tumor destruction may also play a role, such as viral-mediated vascular collapse in the tumor, which has been implicated in anti-tumor activity of several OVs, including those based on vaccinia

(Breitbach et al., 2007, 2013). Further, the use of subcutaneous tumor xenografts minimizes the involvement of stromal cells and matrix in the response, and tumor-associated fibroblasts have recently been implicated in the anti-tumor activity of several OVs, including vaccinia (Ilkow et al., 2015).

This original approach to targeting tumor-induced local defects in the immune system, therefore, appears to be uniquely capable of targeting the highly suppressive MDSC population in the tumor itself. As a result resistant tumors can be sensitized to the immunotherapeutic effects of the viral therapy itself and to other commonly used immunotherapies, such as immune checkpoint blockade. The broad applicability of this approach would be especially exciting in the development of combination immunotherapies that produce more reliable and robust responses in a variety of solid tumors.

EXPERIMENTAL PROCEDURES

Cell Lines, Viruses

A variety of mouse tumor cell lines, including AB12, MOSEC, MC38, CMT93, PAN02, JC, 4T1, B16, CMT TK, Renca, and LLC were used in this research, all were obtained from the American Type Culture Collection, except for MC38 (gift from Dr David Bartlett, University of Pittsburgh), and JC, CMT93, and CMT TK (Cancer Research UK tissue culture collection). All were cultured according to vendors' recommendations. Mouse NKT (CIK) cells were expanded from mouse splenocytes and cultured as previously described (Baker et al., 2001).

The wild-type vaccinia virus Western Reserve (WR) strain was obtained from the American Type Culture Collection (BEI Resources). WR.TK−.Luc$^+$ and WR.B18R$^-$IFNβ$^+$ were described previously (Kirn et al., 2007). WR.TK$^-$HPGD$^+$ and WR.TK$^-$GM-CSF$^+$ were constructed for this work, with the pSC65 plasmid (gift from Prof. Bernie Moss, NIH) cloned to express firefly luciferase from the viral pSE/L promoter and mouse HPGD (or mouse GM-CSF) from the p7.5 promoter. This was recombined into the viral TK gene (see Figure S5). In addition, vvDD.Luc$^+$ and GFP (WR with deletions in TK and the viral growth factor genes, as described previously) was used as a second model of oncolytic vaccinia.

In vitro cell killing was determined by MTS assay of cell survival relative to uninfected controls and plaque assay on lysed cell samples was performed on BSC-1 cell layers.

Animal Models

NOD SCID, C57/BL6, and BALB/c mice (females 6–8 weeks old) were purchased from The Jackson Laboratory. Tumor cells were implanted subcutaneously with 5×10^5 cells injected per mouse. Injection treatments (i.t.) began when tumors reached 50–100 mm^3 (unless otherwise stated). Treatment doses and timings were as indicated. Tumor size was monitored by caliper measurement unless otherwise indicated and mice killed when tumors reached 1,500 mm^3.

Other treatments included the following: anti-PD-1 blocking antibody (BioXCell, RMP1-4) was diluted in PBS and given intraperitoneally (i.p.) at 200 mg/mouse twice weekly; mouse CIK cells were given intravenously at 5×10^6 cell/mouse; anti-PGE$_2$ antibody was given at 20 μg/mouse i.p. daily; celecoxib (Sigma-Aldrich) was given i.p. at 25 mg/kg daily; EP2 (AH6809) and EP4 (AH23848) agonists (both Sigma-Aldrich) were given at 10 mg/kg each daily. Aspirin was given in drinking water ad libitum at doses of 600 μg/ml.

In immune cell-depletion experiments, anti-mouse CD8$^+$ (2.43), anti-mouse CD4$^+$ (GK1.5), or anti-mouse NK1.1 (PK136) (all from BioXCell) were injected i.p. (500 mg) on days 1 and 2 after tumor implantation, with follow-up injections of 150 mg every 5 days thereafter.

In some experiments, tumor homogenates were collected for cytokine and chemokine quantification (by qRT-PCR). Neutralizing antibody titers in serum were determined as described previously (Sampath et al., 2013).

All experiments were performed according to the University of Pittsburgh Institutional Animal Care and Use Committee approved protocols.

Whole-Animal Imaging

In some experiments whole-animal bioluminescence imaging was used to image viral luciferase gene expression. Imaging was carried out on an IVIS 200 (Xenogen, part of PerkinElmer) after i.p. injection of luciferin substrate. Bioluminescence signal was quantified and images analyzed using the Living Image software (Xenogen, part of PerkinElmer). In some other experiments, NKT (CIK) cells were covalently labeled with Cy5.5 NHS Ester (GE Healthcare), and the fluorescence signal was imaged in vivo using the FMT 2500 Fluorescence Whole Animal Imaging System (PerkinElmer). In addition, XenoLight RediJect COX-2 Probe (PerkinElmer) was imaged on the IVIS 200 in vivo.

ELISPOT Assay

IFNγ-producing splenocytes were quantified by ELISPOT assay. Splenocytes were separated from mice after different treatments. Splenocytes were stimulated by lysed tumor cells at a 10:1 ratio or UV-inactivated vaccinia virus at a 5:1 ratio and seeded on plates (EMD Millipore), and coated overnight with 15 ng/mg mIFNγ antibody AN18 (Mabtech). These were incubated for 48 hr before the plates were washed and incubated with a biotinylated secondary antibody R4-6A2-biotin (Mabtech) for 2 hr at room temperature. The plates were then washed, incubated for 1 hr with avidin-peroxidase complex (Vectastatin Kit; Vector Laboratories), and developed by the addition of 3-amino-9-ethylcarbazole (AEC) Substrate Kit (Vector Laboratories) according to the manufacturer's protocol. The spots were counted on a CTL-Immunospot Analyzer (Cellular Technologies). Spots from unstimulated splenocytes from each group were used to subtract the background.

ELISA and Western Blot Assay

Tumor homogenates were harvested from mice treated as indicated, and mechanically disaggregated and digested with triple enzyme mixture (collagenase type IV, DNase type IV, and hyaluronidase type V; Sigma-Aldrich). Serum was collected through sub-mandibular bleed. In vitro cells infected with virus at multiplicity of infection (moi) = 1 for 24 hr or pretreated for 24 hr with 20 nm celecoxib (BioVision) were pretreated with 20 μm arachidonic acid (Sigma-Aldrich) 4 hr before harvest. All experiments were performed in triplicate. Mouse SDF-1(CXCL12), RANTES (CCL5), and I-TAC(CXCL11) ELISAs were performed according to the manufacturer's protocol (Abcam) and PGE$_2$ ELISAs were performed according to the manufacturer's protocol (Cayman Chemical), and optical density was detected using the 3,3,5,5-tetramethylbenzidine (TMB) Peroxidase Substrate Kit (Vector Laboratories).

For western blot assay, in vitro lysed cell protein was prepared. Mouse HPGD antibody (Abcam), COX-2 antibody (BD), and β-actin antibody (Sigma-Aldrich) were used for western blot according to the manufacturer's protocol.

Flow Cytometry

Acquisition was performed on Gallios or Cyan flow cytometers. Data were analyzed using the Cyanor Gallios software. Antibodies included those to CD3, CD4, CD8, CD25, FoxP3, CD11b, Ly6g(Gr-1), Ly6c, CD11b(M1/70), MHC II (M5/114.15.2), CD103 (2×10^7), IL12p40(C17.8) (all BD Biosciences or eBioscience), or CD11c(N418) (BioLegend). Intracellular staining for Foxp3 was done according to protocols in the respective kits. Gating strategies are shown (Figure S3).

In some studies splenocytes were collected and rapidly fixed and permeabilized in order to examine surface markers as well as intracellular stains using Phosflow (including pS6, BD Biosciences).

Quantitative RT-PCR

Total RNA was isolated and purified using an RNeasy Mini Kit (QIAGEN) from whole-tumor homogenates. cDNA was synthesized using a cDNA Synthesis Kit (Quanta BioScience). An array of gene expression assays were performed using a TaqMan Gene Expression Assay following the manufacturer's instructions (reference gene: mouse HPRT) and included IFNγ, CXCL10, CXCL11, lift-1, and lift-2.

Statistical Analysis

Standard Student's t test (two-tailed) were used, with significance considered to be $p < 0.05$.

SUPPLEMENTAL INFORMATION

Supplemental Information includes six figures and can be found with this article online at http://dx.doi.org/10.1016/j.ccell.2016.05.012.

AUTHOR CONTRIBUTIONS

W.H. ran the majority of the experiments described in this work. P.S. ran in vitro viral replication and cell killing assays. J.J.R. constructed novel viral vectors, including VV-HPGD. S.H.T. oversaw the work and wrote the manuscript.

ACKNOWLEDGMENTS

Thanks to Doug Marvel and Rachel Sikorski for help with preparation and running of flow cytometry samples, and David Bartlett and Bernie Moss for providing cell lines and plasmids as indicated. This work was funded by grant support from NIH (R01 CA178766 and R01 CA140215), The Lustgarten Foundation, and through use of CCSG-supported core facilities (P30 CA047904), including animal facilities, In Vivo Imaging Facilities, Flow Cytometry Facility, and Luminex Core. S.H.T. has a financial interest in Western Oncolytics that has licensed this technology.

Received: July 16, 2015
Revised: February 26, 2016
Accepted: May 23, 2016
Published: June 30, 2016

REFERENCES

Alvarez-Breckenridge, C.A., Yu, J., Price, R., Wojton, J., Pradarelli, J., Mao, H., Wei, M., Wang, Y., He, S., Hardcastle, J., et al. (2012). NK cells impede glioblastoma virotherapy through NKp30 and NKp46 natural cytotoxicity receptors. Nat. Med. *18*, 1827–1834.

Andtbacka, R.H.I., Collichio, F.A., Amatruda, T., Senzer, N., Chesney, J., Delman, K.A., Spitler, L.E., Puzanov, I., Doleman, S., Ye, Y., et al. (2013). OPTiM: a randomized phase III trial of talimogene laherparepvec (T-VEC) versus subcutaneous (SC) granulocyte-macrophage colony-stimulating factor (GM-CSF) for the treatment (tx) of unresected stage IIIB/C and IV melanoma. J. Clin. Oncol. *31*, LBA9008.

Baker, J., Verneris, M.R., Ito, M., Shizuru, J.A., and Negrin, R.S. (2001). Expansion of cytolytic CD8(+) natural killer T cells with limited capacity for graft-versus-host disease induction due to interferon gamma production. Blood *97*, 2923–2931.

Breitbach, C.J., Paterson, J.M., Lemay, C.G., Falls, T.J., McGuire, A., Parato, K.A., Stojdl, D.F., Daneshmand, M., Speth, K., Kirn, D., et al. (2007). Targeted inflammation during oncolytic virus therapy severely compromises tumor blood flow. Mol. Ther. *15*, 1686–1693.

Breitbach, C.J., Arulanandam, R., De Silva, N., Thorne, S.H., Patt, R., Daneshmand, M., Moon, A., Ilkow, C., Burke, J., Hwang, T.H., et al. (2013). Oncolytic vaccinia virus disrupts tumor-associated vasculature in humans. Cancer Res. *73*, 1265–1275.

Chatterjee, S., Behnam Azad, B., and Nimmagadda, S. (2014). The intricate role of CXCR4 in cancer. Adv. Cancer Res. *124*, 31–82.

Chen, H., Sampath, P., Hou, W., and Thorne, S.H. (2013). Regulating cytokine function enhances safety and activity of genetic cancer therapies. Mol. Ther. *21*, 167–174.

Donkor, M.K., Lahue, E., Hoke, T.A., Shafer, L.R., Coskun, U., Solheim, J.C., Gulen, D., Bishay, J., and Talmadge, J.E. (2009). Mammary tumor heterogeneity in the expansion of myeloid-derived suppressor cells. Int. Immunopharmacol. *9*, 937–948.

Fujita, M., Kohanbash, G., Fellows-Mayle, W., Hamilton, R.L., Komohara, Y., Decker, S.A., Ohlfest, J.R., and Okada, H. (2011). COX-2 blockade suppresses gliomagenesis by inhibiting myeloid-derived suppressor cells. Cancer Res. *71*, 2664–2674.

Heo, J., Reid, T., Ruo, L., Breitbach, C.J., Rose, S., Bloomston, M., Cho, M., Lim, H.Y., Chung, H.C., Kim, C.W., et al. (2013). Randomized dose-finding clinical trial of oncolytic immunotherapeutic vaccinia JX-594 in liver cancer. Nat. Med. *19*, 329–336.

Ilkow, C.S., Marguerie, M., Batenchuk, C., Mayer, J., Ben Neriah, D., Cousineau, S., Falls, T., Jennings, V.A., Boileau, M., Bellamy, D., et al. (2015). Reciprocal cellular cross-talk within the tumor microenvironment promotes oncolytic virus activity. Nat. Med. *21*, 530–536.

Kalinski, P. (2012). Regulation of immune responses by prostaglandin E2. J. Immunol. *188*, 21–28.

Kim, J.H., Oh, J.Y., Park, B.H., Lee, D.E., Kim, J.S., Park, H.E., Roh, M.S., Je, J.E., Yoon, J.H., Thorne, S.H., et al. (2006). Systemic armed oncolytic and immunologic therapy for cancer with JX-594, a targeted poxvirus expressing GM-CSF. Mol. Ther. *14*, 361–370.

Kirn, D.H., Wang, Y., Le Boeuf, F., Bell, J., and Thorne, S.H. (2007). Targeting of interferon-beta to produce a specific, multi-mechanistic oncolytic vaccinia virus. PLoS Med. *4*, e353.

Kohanbash, G., McKaveney, K., Sakaki, M., Ueda, R., Mintz, A.H., Amankulor, N., Fujita, M., Ohlfest, J.R., and Okada, H. (2013). GM-CSF promotes the immunosuppressive activity of glioma-infiltrating myeloid cells through interleukin-4 receptor-alpha. Cancer Res. *73*, 6413–6423.

Kottke, T., Boisgerault, N., Diaz, R.M., Donnelly, O., Rommelfanger-Konkol, D., Pulido, J., Thompson, J., Mukhopadhyay, D., Kaspar, R., Coffey, M., et al. (2013). Detecting and targeting tumor relapse by its resistance to innate effectors at early recurrence. Nat. Med. *19*, 1625–1631.

Leach, D.R., Krummel, M.F., and Allison, J.P. (1996). Enhancement of antitumor immunity by CTLA-4 blockade. Science *271*, 1734–1736.

Lichty, B.D., Breitbach, C.J., Stojdl, D.F., and Bell, J.C. (2014). Going viral with cancer immunotherapy. Nat. Rev. Cancer *14*, 559–567.

Lun, X.Q., Jang, J.H., Tang, N., Deng, H., Head, R., Bell, J.C., Stojdl, D.F., Nutt, C.L., Senger, D.L., Forsyth, P.A., and McCart, J.A. (2009). Efficacy of systemically administered oncolytic vaccinia virotherapy for malignant gliomas is enhanced by combination therapy with rapamycin or cyclophosphamide. Clin. Cancer Res. *15*, 2777–2788.

Masters, G., Dito, G., Penhallow, B., Lewin, A., Kao, H., and Jure-Kunkel, M. (2014). Antitumor Activity of Anti-PD-1 in Combination with Tyrosine Kinase Inhibitors in a Preclinical Renal Cell Carcinoma Model (San Diego, CA: AACR), p. 5016.

Mastrangelo, M.J., Maguire, H.C., Jr., Eisenlohr, L.C., Laughlin, C.E., Monken, C.E., McCue, P.A., Kovatich, A.J., and Lattime, E.C. (1999). Intratumoral recombinant GM-CSF-encoding virus as gene therapy in patients with cutaneous melanoma. Cancer Gene Ther. *6*, 409–422.

McCart, J.A., Ward, J.M., Lee, J., Hu, Y., Alexander, H.R., Libutti, S.K., Moss, B., and Bartlett, D.L. (2001). Systemic cancer therapy with a tumor-selective vaccinia virus mutant lacking thymidine kinase and vaccinia growth factor genes. Cancer Res. *61*, 8751–8757.

Naik, A.M., Chalikonda, S., McCart, J.A., Xu, H., Guo, Z.S., Langham, G., Gardner, D., Mocellin, S., Lokshin, A.E., Moss, B., et al. (2006). Intravenous and isolated limb perfusion delivery of wild type and a tumor-selective replicating mutant vaccinia virus in nonhuman primates. Hum. Gene Ther. *17*, 31–45.

Obermajer, N., Muthuswamy, R., Lesnock, J., Edwards, R.P., and Kalinski, P. (2011a). Positive feedback between PGE2 and COX2 redirects the differentiation of human dendritic cells toward stable myeloid-derived suppressor cells. Blood *118*, 5498–5505.

Obermajer, N., Muthuswamy, R., Odunsi, K., Edwards, R.P., and Kalinski, P. (2011b). PGE(2)-induced CXCL12 production and CXCR4 expression controls the accumulation of human MDSCs in ovarian cancer environment. Cancer Res. *71*, 7463–7470.

Park, B.H., Hwang, T., Liu, T.C., Sze, D.Y., Kim, J.S., Kwon, H.C., Oh, S.Y., Han, S.Y., Yoon, J.H., Hong, S.H., et al. (2008). Use of a targeted oncolytic poxvirus, JX-594, in patients with refractory primary or metastatic liver cancer: a phase I trial. Lancet Oncol. *9*, 533–542.

Penheiter, A.R., Griesmann, G.E., Federspiel, M.J., Dingli, D., Russell, S.J., and Carlson, S.K. (2011). Pinhole micro-SPECT/CT for noninvasive monitoring

and quantitation of oncolytic virus dispersion and percent infection in solid tumors. Gene Ther. *19*, 279–287.

Rodriguez, P.C., Hernandez, C.P., Quiceno, D., Dubinett, S.M., Zabaleta, J., Ochoa, J.B., Gilbert, J., and Ochoa, A.C. (2005). Arginase I in myeloid suppressor cells is induced by COX-2 in lung carcinoma. J. Exp. Med. *202*, 931–939.

Russell, S.J., Federspiel, M.J., Peng, K.W., Tong, C., Dingli, D., Morice, W.G., Lowe, V., O'Connor, M.K., Kyle, R.A., Leung, N., et al. (2014). Remission of disseminated cancer after systemic oncolytic virotherapy. Mayo Clinic Proc. *89*, 926–933.

Sampath, P., Li, J., Hou, W., Chen, H., Bartlett, D.L., and Thorne, S.H. (2013). Crosstalk between immune cell and oncolytic vaccinia therapy enhances tumor trafficking and antitumor effects. Mol. Ther. *21*, 620–628.

Thorne, S.H., Hwang, T.H., O'Gorman, W.E., Bartlett, D.L., Sei, S., Kanji, F., Brown, C., Werier, J., Cho, J.H., Lee, D.E., et al. (2007). Rational strain selection and engineering creates a broad-spectrum, systemically effective oncolytic poxvirus, JX-963. J. Clin. Invest. *117*, 3350–3358.

Topalian, S.L., Hodi, F.S., Brahmer, J.R., Gettinger, S.N., Smith, D.C., McDermott, D.F., Powderly, J.D., Carvajal, R.D., Sosman, J.A., Atkins, M.B., et al. (2012). Safety, activity, and immune correlates of anti-PD-1 antibody in cancer. N. Engl. J. Med. *366*, 2443–2454.

Tysome, J.R., Li, X., Wang, S., Wang, P., Gao, D., Du, P., Chen, D., Gangeswaran, R., Chard, L.S., Yuan, M., et al. (2012). A novel therapeutic regimen to eradicate established solid tumors with an effective induction of tumor-specific immunity. Clin. Cancer Res. *18*, 6679–6689.

Wang, L.C., Lynn, R.C., Cheng, G., Alexander, E., Kapoor, V., Moon, E.K., Sun, J., Fridlender, Z.G., Isaacs, S.N., Thorne, S.H., and Albelda, S.M. (2011). Treating tumors with a vaccinia virus expressing IFNbeta illustrates the complex relationships between oncolytic ability and immunogenicity. Mol. Ther. *20*, 736–748.

Worschech, A., Chen, N., Yu, Y.A., Zhang, Q., Pos, Z., Weibel, S., Raab, V., Sabatino, M., Monaco, A., Liu, H., et al. (2009). Systemic treatment of xenografts with vaccinia virus GLV-1h68 reveals the immunologic facet of oncolytic therapy. BMC Genomics *10*, 301.

Yuan, J., Gnjatic, S., Li, H., Powel, S., Gallardo, H.F., Ritter, E., Ku, G.Y., Jungbluth, A.A., Segal, N.H., Rasalan, T.S., et al. (2008). CTLA-4 blockade enhances polyfunctional NY-ESO-1 specific T cell responses in metastatic melanoma patients with clinical benefit. Proc. Natl. Acad. Sci. USA *105*, 20410–20415.

Zeh, H.J., Downs-Canner, S., McCart, J.A., Guo, Z.S., Rao, U.N., Ramalingam, L., Thorne, S.H., Jones, H.L., Kalinski, P., Wieckowski, E., et al. (2014). First-in-man study of western reserve strain oncolytic vaccinia virus: safety, systemic spread, and antitumor activity. Mol. Ther. *23*, 202–214.

Zelenay, S., van der Veen, A.G., Bottcher, J.P., Snelgrove, K.J., Rogers, N., Acton, S.E., Chakravarty, P., Girotti, M.R., Marais, R., Quezada, S.A., et al. (2015). Cyclooxygenase-dependent tumor growth through evasion of immunity. Cell *162*, 1257–1270.

Zhang, Q., Yu, Y.A., Wang, E., Chen, N., Danner, R.L., Munson, P.J., Marincola, F.M., and Szalay, A.A. (2007). Eradication of solid human breast tumors in nude mice with an intravenously injected light-emitting oncolytic vaccinia virus. Cancer Res. *67*, 10038–10046.

Zhang, J., Tai, L.H., Ilkow, C.S., Alkayyal, A.A., Ananth, A.A., de Souza, C.T., Wang, J., Sahi, S., Ly, L., Lefebvre, C., et al. (2014). Maraba MG1 virus enhances natural killer cell function via conventional dendritic cells to reduce postoperative metastatic disease. Mol. Ther. *22*, 1320–1332.

Cancer Cell, Volume *30*

Supplemental Information

Oncolytic Virus-Mediated Targeting of PGE_2 in the Tumor Alters the Immune Status and Sensitizes Established and Resistant Tumors to Immunotherapy

Weizhou Hou, Padma Sampath, Juan J. Rojas, and Steve H. Thorne

Supplemental Data

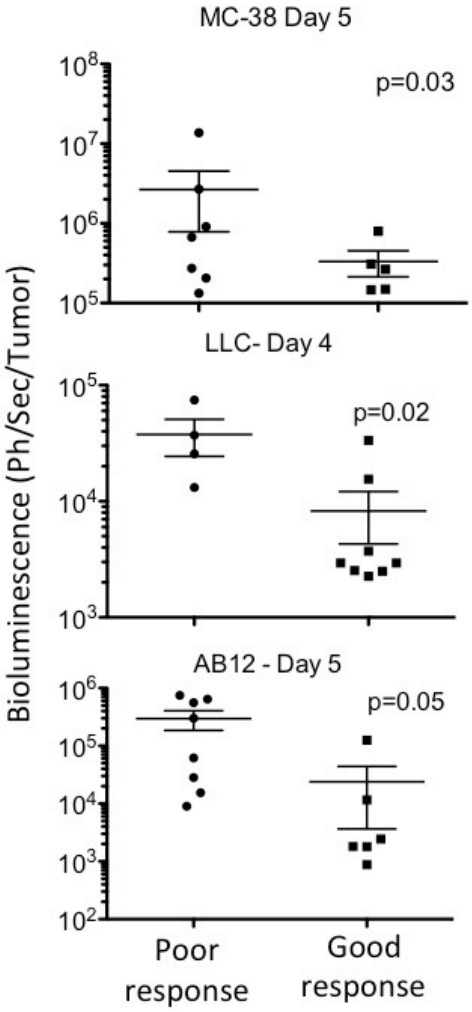

Figure S1, related to Figure 1. Tumor response corresponds to robust viral clearance at day 4/5 after treatment. Bioluminescence (viral luciferase gene expression) was detected on day 4 or 5 after treatment for several subcutaneous tumor–bearing immunocompetent mouse models (MC-38, LLC and AB-12) treated as described in Fig 1B. Within each model individual tumors are divided into good or poor responders and the viral gene expression from the tumor displayed for each group; Error bars ±SEM

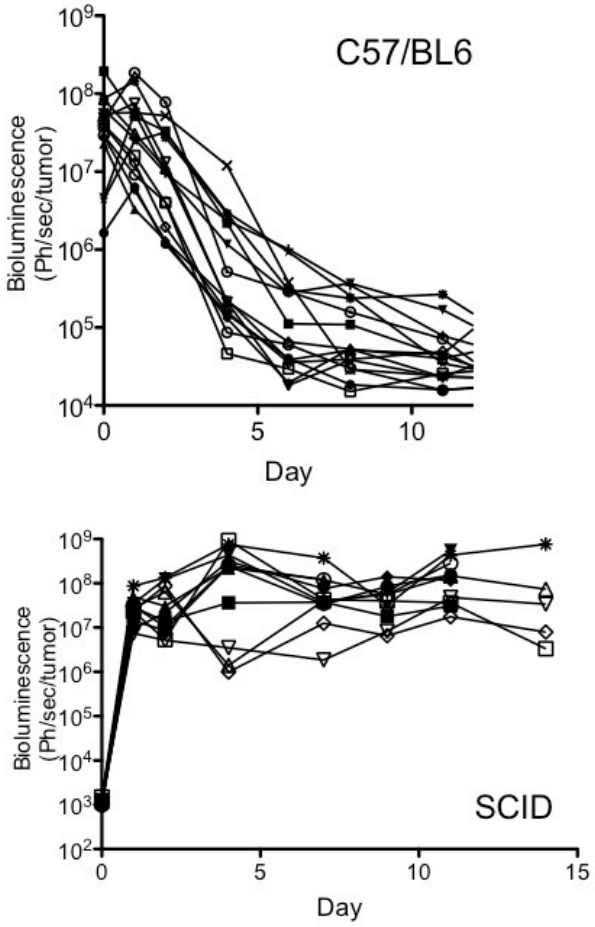

Figure S2, related to Figure 2. Enhanced viral clearance in immunocompetent mice**.** Viral gene expression (luciferase signal) from the tumor for individual mice bearing subcutaneous LLC tumors and treated with $1x10^7$ pfu WR.TK- IT. Immunocompetent (C57/BL6) and immunodeficient (SCID) mice are compared.

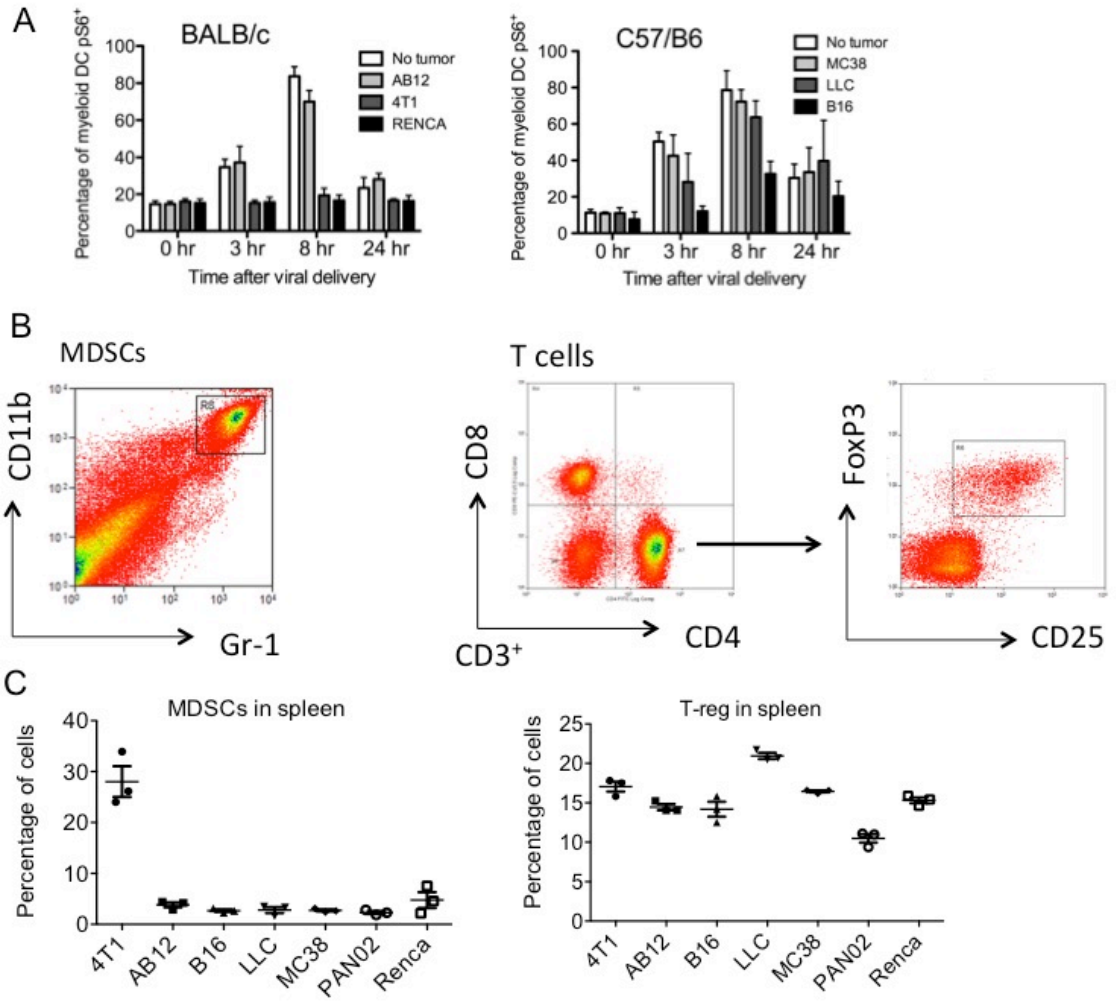

Figure S3, related to Figure 3. Analysis of levels and activation of immune cell subsets in the spleen. **(A)** Splenocytes were collected from mice with indicated tumors (or no tumor) at different times after intravenous (tail vein) injection of $1x10^8$ PFU of WR.TK- (n=3 per time point). Splenocytes were rapidly fixed and permeabilized and stained to examine pS6 levels in myeloid DCs ($CD11c^+CD11b^+B220^-CD8a^-$). 4T1, RENCA and B16 tumors displayed significant reduction ($p<0.05$) in pS6 levels at 3 hr and 8 hr post infection. **(B)** Gating strategies are shown for detection of MDSC (left) and T-cells and T-regs (right) for splenocytes or cells recovered from disaggregated tumors. **(C)** The levels of MDSC and T-reg in the spleen are shown for mice bearing different tumors. Error bars ±SEM

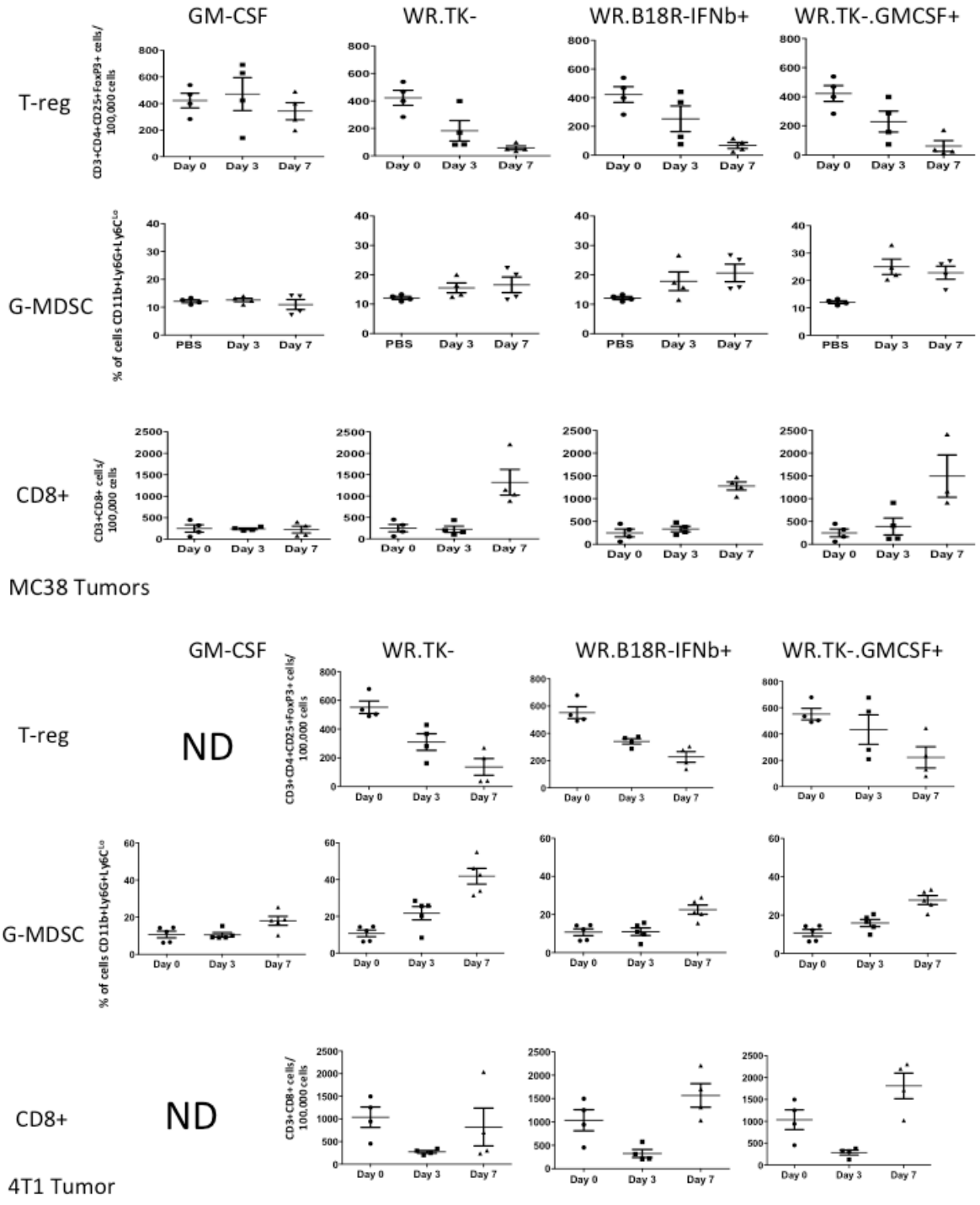

Figure S4, related to figure 3. Effect of different therapies on immune cell profiles in the tumor. Mice bearing MC38 (top) or 4T1 (bottom) tumors were treated and tumors recovered and analyzed as in Fig 2B. Only, in addition to WR.TK-, mice were also treated with recombinant mGM-CSF; WR.B18R-IFNb+; and WR.TK-GMCSF+. Error bars ±SEM

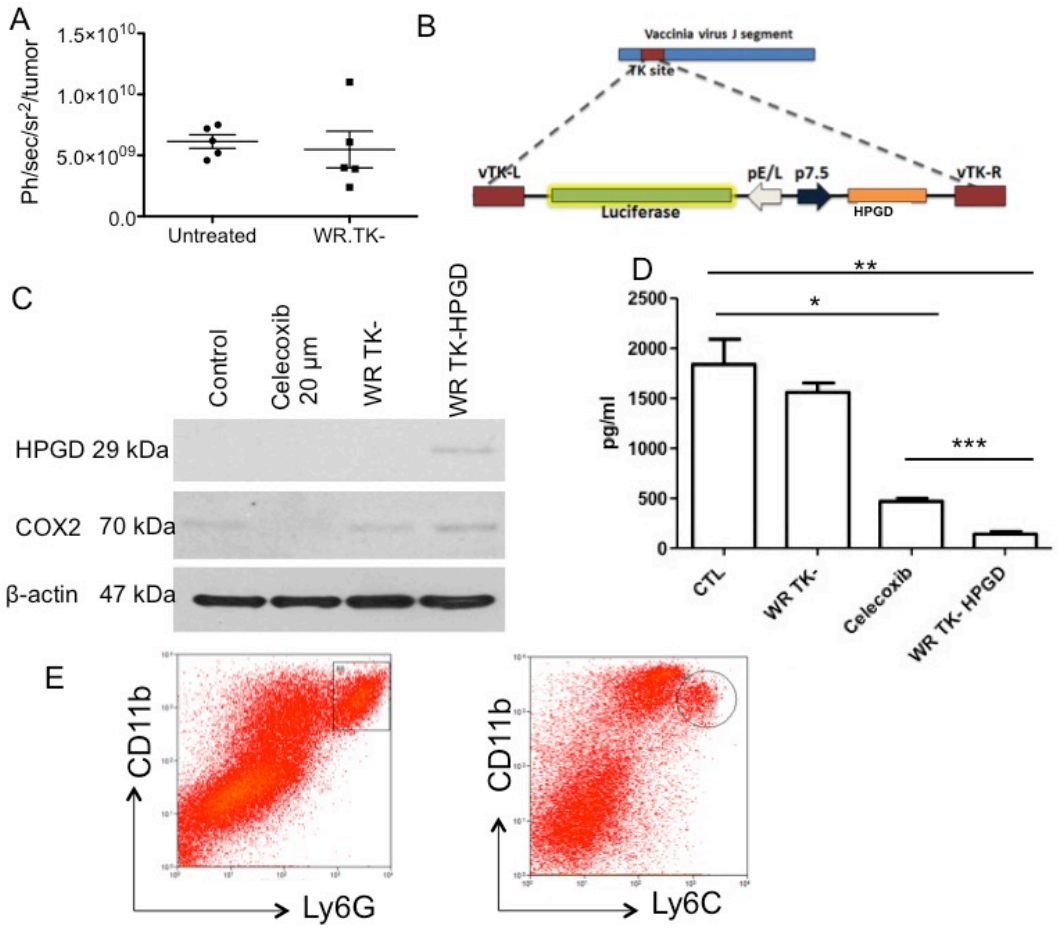

Figure S5, related to Figure 4. Targeting of COX2-PGE_2 pathway with an oncolytic virus to reduce MDSC in the tumor **(A)** Mice (nu-/nu-) bearing Renca tumors were treated with WR.TK- ($1x10^7$ PFU IT) or left untreated (n=5 per group) and COX2 expression was quantified in the tumors after addition of COX2 imaging reagent. Error bars ±SEM. **(B)** Diagram detailing the construction of WR.TK-HPGD+; **(C)** Mouse tumor (Renca) cells were collected 24 hr after infection with WR.TK-, WR.TK-HPGD+ or exposure to 20 µM celecoxib. Cells were treated with arachidonic acid for 4 hr before collection and lysis for Western blotting. Antibodies against HPGD (top), COX2 (middle) and beta-actin were used. **(D)** PGE_2 levels were also determined by ELISA in the media from Renca cells treated as before (* control (CTL) v celecoxib p=0.0017; ** CTL v WR.TK-HPGD+ p=0.0005; *** celecoxib v WR.TK-HPGD+ p=0.0002). Error bars ±SEM. **(E)** Representative plots to demonstrate gating strategy for defining granulocytic (top) and monocytic (bottom) MDSC in the tumor.

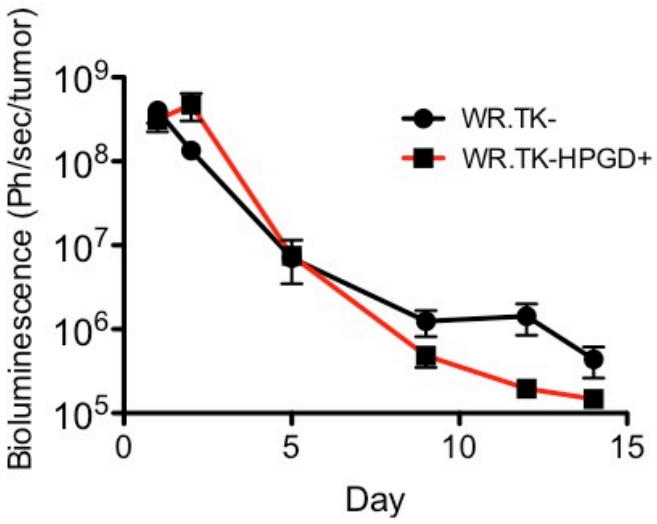

Figure S6, related to figure 5. Viral replication and persistence for vectors with and without HPGD transgene. Average bioluminescence signal from the tumors of mice (BALB/c bearing subcutaneous Renca tumors) after treatment ($1x10^7$ PFU IT) with WR.TK- or WR.TK-.HPGD+ (both expressing luciferase) (n=15 per group). Error bars ±SEM